WING CONFIGURATION EFFECTS ON FLOW FIELD AND AERODYNAMIC PERFORMANCE OF SUPERSONIC BIPLANE FOR SONIC-BOOM REDUCTION

Naoshi Kuratani*, Masahito Yonezawa*, Hiroshi Yamashita*, Shuichi Ozaki*, Toshihiro Ogawa* and Shigeru Obayashi*
*** Institute of Fluid Science, Tohoku University**

Keywords: *Supersonic Biplane, Shock Wace Cancellation, Aspect Ratio, PSP, CFD*

Abstract

The "supersonic biplane theory" is one of the most effective concepts to reduce the sonic boom in supersonic flight. However, the unstart characteristics, that is choking phenomena, was one of the critical issues that disturb the shock wave cancellation between the wings of supersonic biplane. In this study, the shock wave behavior around the wing was visualized and discussed by Schlieren method. And the flow characteristics on the wing were investigated by pressure sensitive paints (PSP) and CFD analysis under the design and off-design Mach number conditions.

These surface pressure profiles on the wing of supersonic biplane clarified that the wave interaction between the oblique shock waves from the leading edge and Mach waves from the wing-tip was dominant of the start/unstart characteristics. Moreover, the two aspect ratio models were used to investigate the effect of aspect ratio on the shock wave interaction and cancellation. The lower aspect ratio achieved the shock wave cancellation, but the higher one did not achieve it under off-design Mach number conditions. The three dimensional flow outward, mainstream Mach number, boundary layer growth on the wing, model dimension and paint thickness were some influencing parameters of start characteristics.

1. Introduction

Recently, the commercial aircrafts have been polarized into large and high-speed types, to fulfill various customer requirements around the world. The former class, represented by aircraft such as the B747, can realize mass transit at low cost for intercontinental transport, and provide superior comfort as in the case of the new A380. On the other hand, since the retirement of Concorde in 2003, the first priority of the latter type is economic efficiency for the airlines, after the Concorde's retirement in 2003. Especially, in order to realize these high-speed aircrafts, environmentally-driven technical issues have to be solved, e.g. noise around airports during take-off and/or landing, and sonic-boom in supersonic flight.

One of the most critical technical issues of supersonic commercial transportation is the sonic boom at supersonic flight that causes large wave drag and impulsive noise to the ground. With regard to aerodynamics, the sonic boom induced by shock waves around the fuselage and the wing is inevitable during supersonic flight. Recently, Kusunose proposed the "supersonic biplane theory" to reduce the sonic boom [3-4]. Briefly, this concept utilizes the shock wave interaction and cancellation between the wings of the Busemann biplane. Adolf Busemann proposed that sonic boom can be reduced by the interaction between shock wave and expansion fan [3-4]. Computational Fluid Dynamics (CFD) analyses [4-8] have been performed to verify this theory. Moreover, CFD analyses and inverse design method [8] have been applied to the supersonic biplane conceptual design and have been shown to produce effective results. However, these methods must be validated by experiment to capture the flow phenomena comprehensively [9-10].

The supersonic biplane has a remarkable advantage during supersonic cruising flight, so

it is a focus of constant attention with regard to the drastic sonic-boom reduction. However, not only the design Mach number performance but also the off-design ones of supersonic biplane must be understood and investigated to realize the supersonic commercial aircraft in the future.

The purpose of this paper was to investigate the fundamental flow characteristics around supersonic biplane at the design and off-design Mach number conditions by supersonic blow-down wind tunnel test facility. Especially, the shock wave patterns and characteristics around supersonic biplane were investigated by Schlieren method. Moreover, the lower wing surface pressure profiles of supersonic biplane were investigated by pressure sensitive paints, PSP and CFD analysis.

2. Supersonic Wind Tunnel Testing

2.1. Supersonic Blow-down Wind Tunnel Facility in ISAS/JAXA

The wind tunnel testing in this paper were conducted in the high speed wind tunnel facility, as shown in Fig. 1, in the Institute of Space and Astronautical Science (ISAS), Japan Aerospace Exploration Agency (JAXA), herein after referred to as ISAS/JAXA. It is an intermittent blow down wind tunnel facility.

This facility can achieve the supersonic and transonic flow conditions. The free-stream Mach number, M_∞, can be changed from 1.5 to 4.0 in the case of supersonic case, and from 0.3 to 1.4 in the transonic case. The free-stream Mach number, M_∞, can be changed by 0.1. The transonic facility can be continuously changed from high to low free-stream Mach number within one wind tunnel operation, which is called Mach-sweep, and hereinafter referred to as M-sweep. It enables the time-series flow measurement around the model.

The test section has 600 mm x 600 mm cross-sectional area and ϕ=600 mm or 400 mm circular windows are installed in the test section for flow visualization. The experimental conditions in this paper are shown in Table 1. The total temperature is the room temperature.

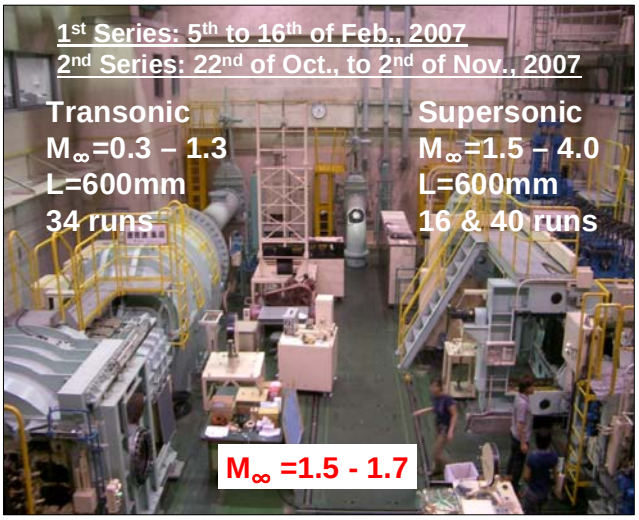

Fig. 1. Overview of Supersonic and Transonic Wind Tunnel Facility in ISAS/JAXA

Table 1. Experimental Conditions for Supersonic Biplane Wind Tunnel Testing.

Test Facility	M_∞[-]	P_0 [MPa]	α [deg.]
Supersonic	1.5, 1.6, 1.7	0.20	0

2.2 Experimental Models

The two different supersonic biplane models, Model-01+ and Model-02, are made of free-cutting stainless steel for a sharp leading-edge, as shown in Fig. 2. These experimental models are used for supersonic wind tunnel testing at ISAS/JAXA. These models have the supporting section downstream, due to being installed with strut. These two-dimensional models were made in order to investigate the flow characteristics between the wings of supersonic biplane and shock wave patterns on the wing surface of supersonic biplane. The coordinate system utilized for the experiment and the CFD results is shown in Fig. 2.

In order to compare with CFD analyses and theoretical studies [3-7], the dimensions of these experimental models have been decided as follows: wing thickness ratio; t/c=0.05. Here, t is the biplane model thickness and c, is the chord length of the biplane. The dimensions of the biplane model were determined by the blockage ratio and the starting load in the supersonic wind tunnel testing. These experimental models have the following dimensions: c=80 mm, t=4 mm and wing span w=60 mm in the case of Model-01+, c=40 mm,

t=2 mm and wing span w=100 mm in the case of Model-02. The interplane distance at the biplane shoulder is G^*=32 mm and the distance at the leading edge is G=40 mm and G/c=0.5 in the case of Model-01+, G^*=16 mm, G=20 mm and G/c=0.5 in the case of Model-02. These configurations of supersonic biplane enable the shock wave interaction and cancellation between the wings of supersonic biplane at design Mach number M_∞=1.7, according to theoretical and Euler calculations [3-7].

The aspect ratio of AR=0.75 in the case of Model-01+ is smaller than the standard two-dimensional wing model in order to reduce the starting load in this wind tunnel testing. The standard aspect ratio is more than 1.5 to avoid the effect of Mach cones from both wing tips on the surface of the biplane. The previous CFD analyses [5, 7] were usually conducted under the aspect ratio AR=4.0. Therefore, Model-02 has higher aspect ratio AR=2.50 than that of Model-01+ to investigate the effect of the aspect ratio on the flow characteristics. These model specifications are summarized in Table 2.

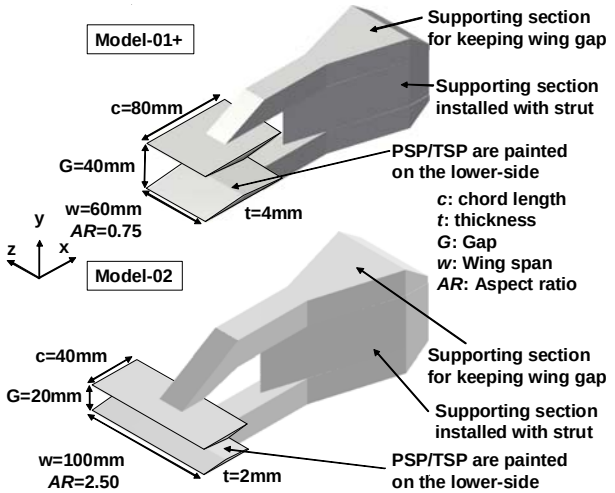

Fig. 2. Supersonic Biplane Experimental Models

Table 2. Specifications of Supersonic Biplane Experimental Models

Model	c mm	t mm	G mm	G^* mm	w mm	AR -
-01+	80	4	40	32	60	0.75
-02	40	2	20	16	100	2.50

2.3. Schlieren Flow Visualization

Schlieren flow visualization around the supersonic biplane experimental model was performed in supersonic flow conditions. Two parabolic with focal length 6 m and two planar mirrors for Schlieren system are set up to enhance the flow visualization images by a long optical path length. The continuous light source is the Xenon flash lamp. These Schlieren photographs were captured by standard video camera at 30 Hz and used for monitoring the test section condition during wind tunnel operation from the remote control room.

2.4. Surface Pressure Measurement

2.4.1 Pressure and Temperature Sensitive Paint (PSP/TSP)

In this study, pressure sensitive paint, PSP, was used for surface pressure measurement in order to investigate the shock wave patterns on the lower wing of supersonic biplane model. PSP is a coating-type molecular sensor that consists of luminescent molecules and polymer binder. These molecules are excited electronically to an elevated energy state, when illuminated with light at a certain wavelength. These excited molecules return to the ground state through several photochemical mechanisms; radiative decay (luminescence), non radiative decay (heat release) and oxygen quenching. The principle of PSP measurement is based on oxygen quenching. These oxygen molecules in the air around PSP absorb the excited energy of sensor molecules, and luminescent intensity decreases. The luminescent intensity is proportional to oxygen partial pressure in the air around the sensor. Moreover, the luminescent intensity is influenced by temperature. The effect of temperature must be corrected to measure pressure precisely and quantitatively. The relationship between the luminescent intensity I and pressure P is theoretically expressed by Stern-Volmer relation as follows;

$$\frac{I(P_{ref},T)}{I(P,T)} = A(T) + B(T)\frac{P}{P_{ref}} \qquad (1)$$

Where the subscript *ref* represents the reference condition, and $A(T)$ and $B(T)$ are calibration coefficients. Note that these coefficients are functions of temperature T. Using Eq. (1), the surface pressure P can be calculated from the

ratio of luminescent intensity images between the wind-on and wind-off (reference) conditions.

However, the temperature at the wind-on condition is different from that at the wind-off condition in the case of actual conditions. That is, PSP depends not only on the pressure but also on the temperature. Therefore, it is necessary to correct the effect of temperature to calculate the accurate surface pressure. In this study, Eq. (1) is transformed to the following expression [10].

$$\frac{I(P_{ref},T_{ref})}{I(P,T)} = \alpha(T)\cdot\left(A(T)+B(T)\frac{P}{P_{ref}}\right) \qquad (2)$$

Where $\alpha(T) = I(P_{ref}, T_{ref})/I(P_{ref}, T)$. This factor is called as the temperature correction factor.

In this paper, UF470 (ISSI Inc.) is used as PSP. This PSP is composed of PtTFPP as luminophore, FIB as binder, Benzene as solvent and TiO_2 as scattering agent. This paint emits the phosphorescence with a peak wavelength of 650nm by 405nm excited light. The UF470 is "ideal" paint that means the coefficients, $A(T)$ and $B(T)$, are independent of temperature. Therefore, only the effect of temperature on $\alpha(T)$ in Eq. (2) should be taken into account in the case of UF470 paint. In this paper, $\alpha(T)$ is evaluated by using a Temperature Sensitive Paint (TSP) measurement conducted in different runs.

TSP is also a coating-type sensor like PSP, consisting of sensor molecules and polymer binder. In contrast to PSP, the sensor molecules in TSP cause no oxygen quenching, but have relatively high activation energy for non-radiative decay. The luminescent intensity of TSP decreases with increasing temperature according to Arrhenius equation. For practical purposes, these characteristics can be expressed by the following polynomial equation;

$$\frac{I(T)}{I(T_{ref})} = \sum_{i}^{2} a_i \left(\frac{T}{T_{ref}}\right)^i \qquad (3)$$

Where a_i are the coefficients determined by calibration test. This TSP is composed of $Ru(phen)_3^{2+}$(dichlorotris-(1,10- phenanthroline)--ruthenium(II)-hydrate) as luminophore, Poly-acrylic acid as binder, Ethanol as solvent and FB-200 (ISSI Inc.) as basecoat. $Ru(phen)_3^{2+}$ have a high temperature sensitivity around room temperature. The peak excitation spectra are about 350, 430-450 nm and the emission peak spectrum is about 610 nm.

2.4.2 Optical Setup

An optical setup for PSP and TSP measurement is shown in Fig. 5. The excitation light source was two UV-LED units with a peak emission wavelength of 395nm. To cut undesirable near-infrared excitation light, a "band-passed filter" which could transmit light with the wavelength of 400±50nm was placed in front of UV-LED unit. Luminescent intensity images for PSP or TSP were acquired using a 12bit cooled CCD camera (Hamamatsu, C4742-98). The CCD camera spatial resolution is 1024×1024 pixels. Either of a band-passed filter, which could be made to pass the wavelength of 650±20nm, or a high-pass filter, which could be made to pass the wavelength of over 580nm, was placed in front of CCD camera lens for PSP and TSP, respectively, in order to cut the excitation lights emitted from LED units. The sequential 20 wind-on images were acquired during wind tunnel operation and the exposure time is 620 ms.

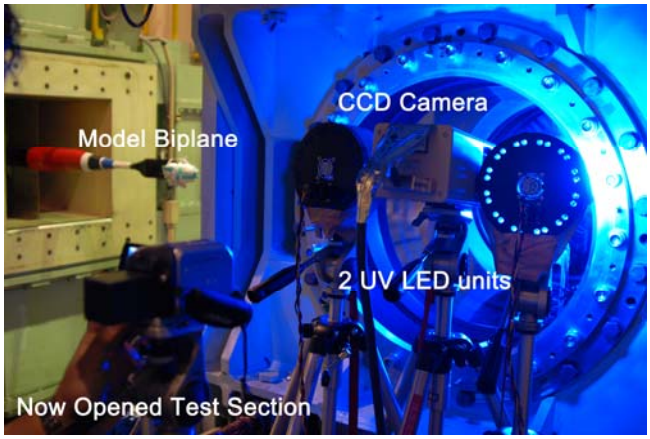

Fig. 5. Photograph of Optical Setup for PSP/TSP Measurement

2.4.3 Data Processing Procedure

The wind-off images, that is, reference images I_{ref}, were captured before wind tunnel starts. 10 reference images were captured and averaged to reduce shot and read-out noises. A sequential 20 wind-on images were captured during wind tunnel runs. These wind-on images can be categorized as the images captured during the wind tunnel starting process, the ones during effective wind tunnel runs and the ones after the

wind tunnel stopped. Here, these images just before the wind tunnel stops are called as I_{run} and the images just after it stops called as I_{ref_after}. For PSP measurement, I_{ref_after} was used as the reference image, because this procedure can reduce the influence of temperature, according to [10], when the temperature distribution at the wind-on condition is maintained at constant immediately after the wind tunnel stops. TSP measurement was, therefore, performed to confirm the temperature distribution during wind tunnel runs.

These luminescent images for PSP and TSP were analyzed as following process, as shown in Fig. 6; ensemble averaging of 10 images, subtraction the background dark current images from raw images, registration of the wind-on and wind-off images, calculation of luminescent intensity ratio, conversion of the ratio to pressure or temperature absolutely using a-priori method including the coefficients obtained by a calibration chamber and paint samples, and finally correction of temperature by multiplying the temperature correction factor $\alpha(T)$, calculated from temperature measured by thermocouple and/or TSP.

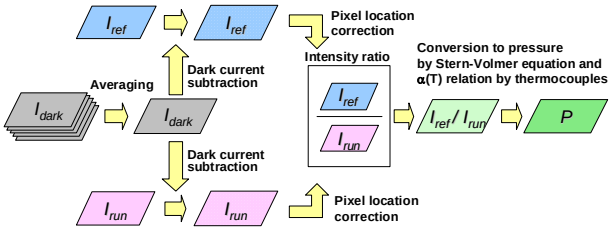

Fig. 6. Image Processing Procedure for PSP/TSP Measurement

2.5. Computational Method

A three-dimensional unstructured flow solver named TAS code (Tohoku University Aerodynamic Simulation code) [15] using three dimensional unstructured grid is performed to investigate the supersonic and transonic flow around the biplane. Navier-Stokes equations are solved by a finite-volume cell-vertex scheme. A hybrid volume grid composed of tetrahedrons, prisms, and pyramids is used for Navier-Stokes computations. The numerical flux is computed using the approximate Riemann solver of Harten-Lax-van Leer-Einfeldt-Wada (HLLEW) [16]. The second order spatial accuracy is realized by a linear reconstruction of the primitive gas dynamic variables with Venkatakrishnan's limiter. The lower/upper symmetric Gauss-Seidel (LU-SGS) implicit method for unstructured mesh [17] is used for the time integration. The one-equation turbulence model [18] by Spalart-Allmaras is introduced to treat the turbulent boundary layers and solve the Navier-Stokes equations.

3. Results and Discussion

3.1. Shock Wave Visualization

3.1.1 Shock Wave Interaction and Cancellation at Design Mach number, M_∞=1.7

Supersonic wind tunnel testing were performed at a design Mach number, M_∞=1.7, by high speed wind tunnel facility in ISAS/JAXA, in order to investigate the shock wave interaction and cancellation by supersonic biplane. These biplane model configuration with area ratio, G^*/G=0.8, cannot be satisfied with quasi one-dimensional criterion, that is, Kantrowitz-Donaldson criterion [11-14] at a design Mach number [6]. Consequently, these experimental biplane models, as shown in Fig. 2, are predicted to not start, that is, shock wave interaction and cancellation between the wings of the supersonic biplane could not be achieved.

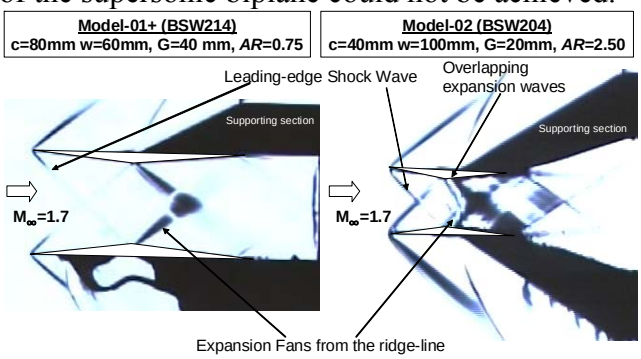

Fig. 6. Schlieren Photographs of Shock Wave Interaction and Cancellation between the Wings of Supersonic Biplane at Design Mach number, M_∞=1.7 (Model-01+ and Model-02)

However, these Schlieren photographs, as shown in Fig. 6, shows the shock wave interaction and cancellation between the wings

of supersonic biplane at M_∞=1.7. These oblique shock waves from the leading edge of wings reached the ridgeline of the opposite side wing, and the expansion fans were propagated from the ridgeline of biplane. It is believed that the higher pressure between the wings due to the shock waves propagating from the leading edge of wings caused the spill out of the biplane. The static pressure outside of biplane is lower than that between the wings due to the free-stream supersonic flow. Such a three-dimensional flow effect results in the avoidance of the unstart characteristics.

Especially, the darkened expansion fans were visualized due to the higher pressure gradient as shown in Fig. 6. The remarkable difference between these images was the darkened area downstream of the ridgeline due to the overlapped expansion fans. The flow visualization area in the case of Model-02 was emphasized due to the smaller field view and longer light path in the spanwise direction. Because the wing span of Model-02 is 1.67 times length as that of Model-01+ and the gap between the wings of Model-02 is half width as that of Model-01+.

3.1.2 Shock Wave Behaviors at Off-design Mach numbers, M_∞=1.6 and 1.5

In addition, the supersonic wind tunnel testing were conducted at off-design Mach numbers M_∞=1.5 and 1.6 smaller than M_∞=1.7 in order to find out at which Mach number the unstart occurred. These Schlieren photographs in the cases of Model-01+ and Model-02 are shown in Fig. 7 at M_∞=1.6 and in Fig. 8 at M_∞=1.5. At first, Schlieren photographs, as shown in the left side images in Fig. 7 and 8, are focused in the case of Model-01+. These oblique shock angles at the leading edge of biplane are gradually larger at a Mach number smaller than M_∞=1.7. As results, these shock waves reached the upstream of the ridgeline as shown in Fig. 7 and 8. They gradually reached at upstream of the ridgeline of biplane with the decrease in Mach number. However, these shock wave interaction and cancellation were not shifted to unstart condition due to the three-dimensional flow effect as mentioned in the case of Model-01+. These oblique shock waves reflected by the opposite sides of wing, and the expansion fans from the ridgeline interacted, and resulted in the complicated supersonic flow field between the wings of supersonic biplane.

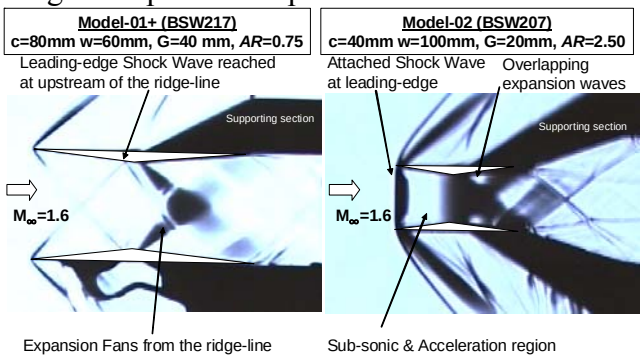

Fig. 7. Schlieren Photographs of Shock Wave Visualization around Supersonic Biplane at Off-design Mach number, M_∞=1.6 (Model-01+ and Model-02).

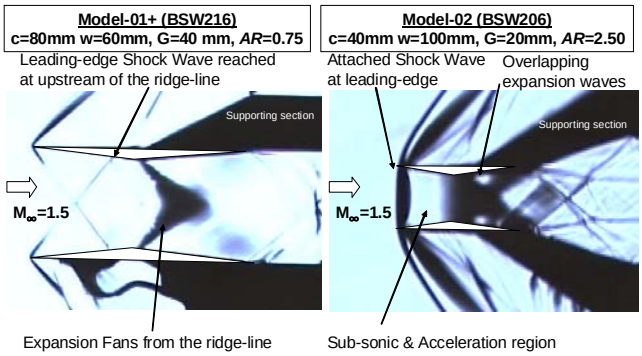

Fig. 8. Schlieren Photographs of Shock Wave Visualization around Supersonic Biplane at Off-design Mach number, M_∞=1.5 (Model-01+ and Model-02).

Meanwhile, Schlieren photographs, as shown in the right side images in Fig. 7 and 8, are focused in the case of Model-02. The remarkable difference between these images was the unstart, that is, the attached shock wave at leading edge of biplane, as shown in Fig. 7 and 8. The oblique shock waves from the leading edge could not be swallowed and that caused the strong attached normal shock wave at the leading edge. It is believed that the three dimensional flow effect of Model-02 was not stronger than that of Model-01+ due to the longer wing span. Moreover, these attached shock waves resulted in the subsonic flow behind the shock waves and the subsonic flow was accelerated from the leading edge to the ridgeline of biplane, because the biplane was performed as the subsonic nozzle. The darkened area downstream of the ridgeline was accelerated to supersonic flow by the expansion

fans. And the slip lines were developed from the discontinuous plane area at the trailing edge of biplane and the waves from the boundary area with mainstream were clearly visualized downstream of the supersonic biplane.

3.2. Surface Pressure Distribution by PSP Measurement

3.2.1 Shock Wave Patterns on the Lower Wing of Supersonic Biplane, M_∞=1.7

In above mentioned sections, the shock wave visualization was performed to investigate the shock wave patterns around the supersonic biplane; however, it is difficult to clarify the three dimensional flow fields around it.

Moreover, PSP measurement was performed to investigate the shock wave patterns on the lower wing surface of supersonic biplane at design Mach number condition M_∞=1.7. The lower wing of supersonic biplane was focused on, because there were the symmetric pressure profiles on the both sides of supersonic biplane at an angle of attack of 0 degree. These PSP images are shown in Fig. 9, and the left side image is Model-01+ case and the right one is Model-02 case.

These images clarified the detailed shock wave patterns on the lower wing surface. In the case of Model-01+, the shock wave interaction and cancellation was achieved, as shown in Fig. 9. There was the spatially homogenous pressure distribution downstream of the leading edge, however, there was Mach waves from the wing tips and they interacted with the oblique shock waves from the leading edge and caused the lower surface pressure inside of Mach waves. The higher pressure region was the convex pressure region upstream of the ridgeline. This was why there was the regular intersection with the oblique shock waves from the leading edge of upper- and lower wings along the centerline of wing and the higher pressure region outward of wing was strongly affected by Mach waves.

There was the lower pressure region at the downstream of x/c=0.8 due to the expansion waves and fans from the ridgeline. At around x/c=0.8 there was spanwise line that means the reflected shock wave from the upper wing. And the rearward wings were performed as supersonic nozzle downstream of supersonic biplane and the flow between the rearward wings was accelerated.

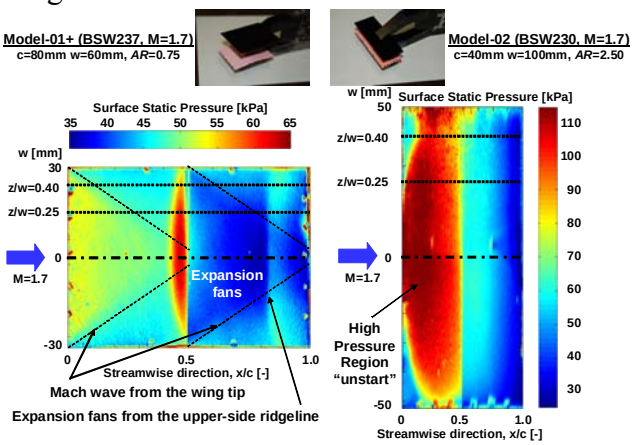

Fig. 9. Surface Pressure Distribution on the Lower Wing of Supersonic Biplane by PSP Measurement at Design Mach number, M_∞=1.7 (Model-01+ and Model-02).

Meanwhile, in the case of Model-02, there was significantly different surface pressure profile compared with Model-01+ case, as shown in Fig. 9. There was the broad convex higher pressure region upstream of the ridgeline due to the wing gap and span. Compared with Model-01+, the two-dimensional flow between the wings was dominant in the case of Model-02. Therefore, the flow condition between the wings seemed to be transited to the unstart condition.

However, the Schlieren image, as shown in Fig. 6, showed the start condition in the case of Model-02. There was the remarkable difference between the Schlieren and PSP images. Although these models have same area ratio based on Kantrowitz-Donaldson Criterion, there were different surface pressure profiles. It is believed that this difference was affected by the small changes in the mainstream Mach number, the boundary layer growth on the wing surface, the model dimensions and the thickness of paints on the wing. These effects of the parameters on the start characteristics must be clarified and understood to maintain the start.

3.2.2 Shock Wave Patterns on the Lower Wing of Supersonic Biplane, M_∞=1.6 and 1.5

In addition, PSP measurement was performed to investigate the shock wave patterns on the lower wing of supersonic biplane at the off-design Mach number conditions M_∞=1.6 and 1.5. These

PSP images are shown in Fig. 10 and 11 respectively, and the left side images are Model-01+ cases and the right ones are Model-02 cases.

In the case of Mode-01+, PSP image at M_∞=1.6 was almost similar to that at M_∞=1.7 as shown in Fig. 10. The decrease in mainstream Mach number affected the increase in the shock angle of the oblique shock at the leading edge and the increase in Mach angle of Mach wave from the wing tip, and resulted in the larger convex pressure region upstream of the ridgeline than that in the case of Model-01+. And the higher pressure region of the ridgeline was larger with the decrease in mainstream Mach number due to the increase in shock angle at the leading edge as shown in Fig. 11.

On the other hand, the concave higher pressure region was visualized with the decrease in mainstream Mach number in the case of Model-02 as shown in Fig. 10 and 11. It's highly possible that these shock wave patterns showed the start/unstart transition between M_∞=1.6 and 1.7. The higher pressure region was changed from the convex to the concave with the decrease in mainstream Mach number. This change in the higher pressure region seemed to blow out the oblique shock waves from the leading edge without the swallowing.

Moreover, as shown in Fig. 11, there was similar concave higher pressure region under M_∞=1.5 in the case of Model-02. This transition must be investigated to control the unstart/start condition.

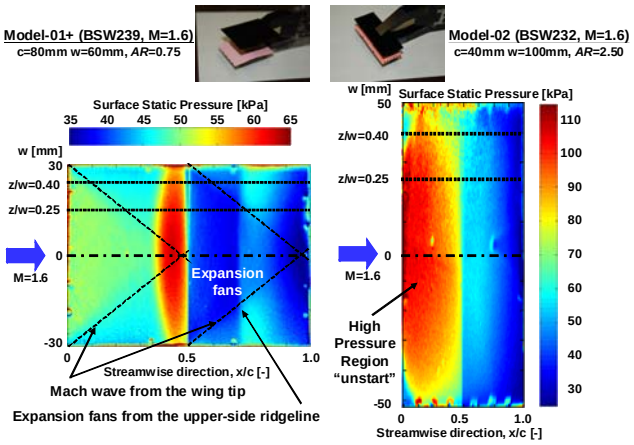

Fig. 10. Surface Pressure Distribution on the Lower Wing of Supersonic Biplane by PSP Measurement at Off-design Mach number, M_∞=1.6 (Model-01+ and Model-02).

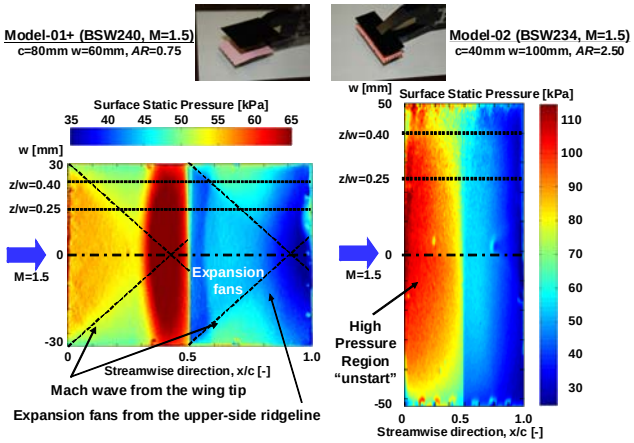

Fig. 11. Surface Pressure Distribution on the Lower Wing of Supersonic Biplane by PSP Measurement at Off-design Mach number, M_∞=1.5 (Model-01+ and Model-02).

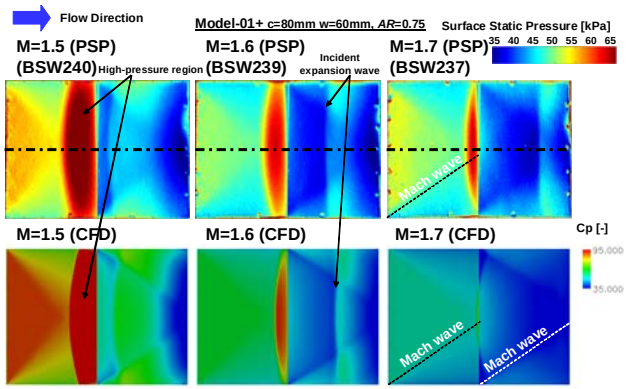

Fig. 12. Surface Pressure Distribution on the Lower Wing of Supersonic Biplane by PSP Measurement and CFD analysis at M_∞=1.5-1.7 (Model-01+).

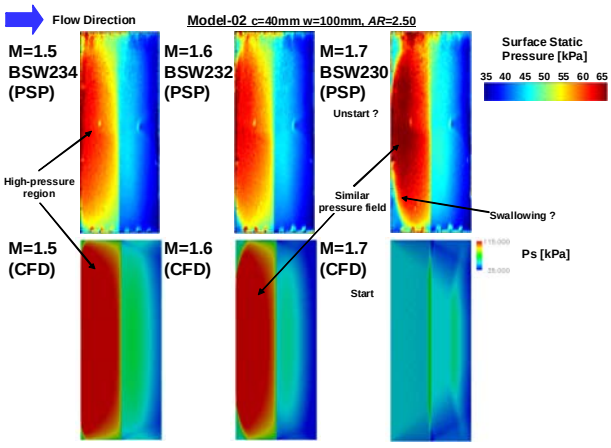

Fig. 13. Surface Pressure Distribution on the Lower Wing of Supersonic Biplane by PSP Measurement and CFD analysis at M_∞=1.5-1.7 (Model-02+).

3.3. PSP and CFD Comparison for Lower Wing Surface Pressure Field

In above mentioned sections, the shock wave visualization was performed to investigate the shock wave patterns around the supersonic biplane; however, it is difficult to clarify the three dimensional flow fields around it. Here CDF analysis was performed to compare with the lower wing surface pressure field, as shown in Fig. 12 and 13. There were similar surface pressure patterns of Model-01+ between PSP images and CFD analysis as shown in Fig. 12. Qualitative flow characteristics can be discussed by CFD analysis, too.

On the other hand, in the case of Model-02, there were slight different pressure fields between PSP images and CFD analysis as shown in Fig. 13. The PSP results clarified the shape of the higher pressure region upstream of the ridgeline changed from the convex to the concave with the decreasing mainstream Mach number. The attached normal shock wave caused the transition from the start to unstart. And there were similar lower surface pressure between the PSP image at M_∞=1.7 and CFD result at M_∞=1.6. CFD analysis was performed at the theoretical and steady conditions. Therefore, these differences between M_∞=1.6 and 1.7 were caused by the small changes in the mainstream Mach number, the boundary layer growth on the wing surface, the model dimensions and the thickness of paints on the wing and so on.

4. Conclusions

The supersonic wind tunnel testing were performed to investigate the flow characteristics around the supersonic biplane models with two different aspect ratios and M_∞=1.5 to 1.7. Consequently, Schlieren photographs showed the shock wave characteristics around the supersonic biplane. PSP measurement and CFD analysis play an essential role in understanding of the shock wave and flow characteristics in detail. The conclusions that can be drawn from this study are as follows:

1) Shock wave interaction and cancellation was experimentally achieved at a design Mach number, M_∞=1.7 in the both cases of Model-01+ and Model-02. The interaction region by the oblique shock waves from the leading edge and Mach waves from the wing tip was dominant of start characteristics.
2) In the case of lower aspect ratio model, shock wave interaction and cancellation was experimentally achieved under off-design Mach numbers, too. Because a three-dimensional flow effect outward due to the pressure difference resulted in the avoidance of the transition to the unstart condition.
3) In the case of higher aspect ratio model, shock wave interaction and cancellation was not experimentally achieved under off-design Mach numbers. The following parameters on the unstart condition must be clarified: the small changes in the mainstream Mach number, the boundary layer growth on the wing surface, the model dimensions and the thickness of paints on the wing and so on.

Acknowledgements

The authors would like to thank Dr. Tomoko Irikado and Dr. Akira Oyama of the Institute of Space and Astronautical Science, the Japan Aerospace Exploration Agency (ISAS/JAXA) for considerable supports for executing the wind tunnel testing. The authors also would like to thank Prof. Keisuke Asai, Dr. Hiroki Nagai and Mr. Soshi Oyama at Department of Aerospace Engineering, Tohoku University, for considerable supports for executing PSP measurement.

This study is supported by Grant-in-aid scientific research (No. 19206086), Ministry of Education, Culture, Sports, Science and Technology in Japan, “Silent Supersonic Transportation Workshop” of Aerodynamic Division Committee, The Japan Society for Aeronautical and Space Sciences, and 21st Century COE Program “International COE of Flow Dynamics”, Institute of Fluid Science, Tohoku University.

References

[1] Kusunose K. A New Concept in the Development of Boomless Supersonic Transport. *1st International Conference on Flow Dynamics,* Sendai Japan, pp.46-47, 2004.

[2] Yonezawa M, Yamashita H, Obayashi S and Kusunose K. Investigation of Supersonic Wing Shape Using Busemann Biplane Airfoil. *The 45th AIAA Aerospace Sciences Meeting and Exhibit*, Reno USA, AIAA-2007-0686, 2007.

[3] Yamashita H and Obayashi S. Numerical Investigation on Sonic Boom Reduction with Non-axisymmetric Body Shapes. *The 46th AIAA Aerospace Sciences Meeting and Exhibit*, Reno USA, AIAA-2008-59, 2008.

[4] Maruyama D, Matsushima K, Kusunose K and Nakahashi K. Aerodynamic Design of Three-Dimensional Low Wave-Drag Biplanes Using Inverse Problem Method. *The 46th AIAA Aerospace Sciences Meeting and Exhibit*, Reno USA, AIAA-2008-289, 2008.

[5] Kusunose K. et al. *Aerodynamic Design of Supersonic Biplane: Cutting Edge and Related Topics*. Tohoku University Press, Volume 5. 2007.

[6] Kuratani N, Ogawa T, Yamashita H, Yonezawa M and Obayashi S, Experimental and Computational Fluid Dynamics around Supersonic Biplane for Sonic-Boom Reduction, *The 13th AIAA/CEAS Aeroacoustics Conference (The 28th AIAA Aeroacoustics Conference)*, Rome Italy, AIAA 2007-3674, 2007.

[7] Kuratani N, Ogawa T, Yonezawa M, Yamashita H and Obayashi S. Aerodynamic Performance of Supersonic Biplane for Sonic-Boom Reduction, *Fourth International Conference on Flow Dynamics*, Sendai Japan, No. 3-4-5, 2007.

[8] Saito K, Nagai H, Ogawa T and Asai K. Development of Pressure-Sensitive Paint Technique in a Supersonic Indraft Wind Tunnel and its Application to a Busemann Biplane, *22nd International Congress on Instrumentation in Aerospace Simulation Facilities*, Pacific Grove, California, 2007.

[9] Saito K, Nagai H, Ogawa T and Asai K. Experimental Study on Interference Flow of a Supersonic Busemann Biplane, *39th Fluid Dynamics Conference / Aerospace Numerical Simulation Symposium 2007,* Tokyo Japan, pp.13-14, 2007. (in Japanese)

[10] Yamashita T, Sugiura H, Nagai H, Asai K and Ishida K. Pressure-Sensitive Paint Measurement of the Flow around a Simplified Car Model, *12th International Symposium on Flow Visualization*, Gottingen Germany, 2006-67.4(259), 2006.

[11] Van Wie D M, Kwok F T, Walsh R F. Starting Characteristics of Supersonic Inlet *32nd AIAA/ASME/SAE/ASEE Joint Propulsion Conference*, AIAA 96-2914, Lake Buena Vista FL, 1996.

[12] Van Wie D M, White M E, Waltrup P J. Application of Computational Design Techniques in the Development of Scramjet Engines *19th AIAA Fluid Dynamics, Plasma Dynamics and Lasers Conference*, AIAA 87-1420, Honolulu HI, 1987.

[13] Van Wie D M, Molder S. Applications of Busemann Inlet Designs for Flight at Hypersonic Speeds *AIAA Aerospace Design Conference*, AIAA 92-1210, Irvine CA, 1992.

[14] Molder S, Szpiro E J. Busemann Inlet for Hypersonic Speeds *Journal of Aircraft*, Vol.3, No.8, pp.1303-1304, 1996.

[15] Ito Y, Nakahashi K. Unstructured Mesh Generation for Viscous Flow Computations *Proceedings of the 11th International Meshing Roundtable*, Ithaca, NY, pp. 367–377, 2002.

[16] Obayashi S, Guruswamy G. P. Convergence Acceleration of an Aeroelastic Navier-Stokes Solver *AIAA Journal*, Vol. 33, No. 6, pp. 1134-1141, 1994.

[17] Sharov D, Nakahashi K. Reordering of Hybrid Unstructured Grids for Lower-Upper Symmetric Gauss-Seidel Computations, *AIAA Journal*, Vol. 36, No. 3, pp. 484-486. 1998.

[18] Spalart P. R, Allmaras S. R. A One-Equation Turbulence Model for Aerodynamics Flows, *30th AIAA Aerospace Sciences Meeting and Exhibit*, Reno, 1992, January, AIAA Paper 92-0439. 1992.

Copyright Statement